Depth analysis of planar array for 3D electrical impedance tomography

Bo Chen, Manuchehr Soleimani

***Abstract*—EIT imaging modality has great potential on industrial applications with the advantages of being high temporal resolution. It is especially useful in cases, such as, geophysical detection, landmine detection and detections on non-transparent region, where measurement data is only available from single surface, for data acquisition. Instead of the circular EIT model that uses the traditional circular electrode model, in this work, planar array EIT is implemented, aiming to visualize a pipeline transporting a two-phase flow. The planar array can explore spatial information within its detectable region by producing 3D images, which have a higher spatial resolution in axis-direction than a traditional EIT with a dual-plane electrode sensor. However, in solving the inverse problem of a 3D subsurface EIT using a planar array the images may be degraded, especially in cases where the location of the target is relatively deep. The total variation (TV) algorithm as block prior assumption based regularization method has the potential to improve the image quality, and some works have shown that TV reconstructs sharper images, which provides an advantage when representing spatial information. In this chapter, the performance of subsurface EIT using the TV algorithm for 3D visualization are presented based on simulations and experiments, and the results of quantitative measurement of depth are discussed.**

***Index Terms*—Electrical resistance tomography, image reconstruction, total generalized variation.**

I. INTRODUCTION

Electrical impedance tomography (EIT) is capable of visualizing tested samples by solving conductivity distribution based on forward modelling and solving the inverse problem. The solution of forward problem is achieved by combining FEM with the complete electrode model, and EIDORS is a useful tool in the forward modelling of EIT. Various algorithms have been invented for image reconstruction to solve the inverse problem, where regularization is involved to overcome the trouble brought by the ill-pose nature of EIT inverse problem. Linear back projection (LBP) is an early-proposed algorithm [1], where the inversed Jacobian J^{-1} is approximated by its transpose J^T to make the calculation, consequently, poor image-quality visualizations were created. Regularization of EIT is an optimization problem, and most regularization methods are classified as l2-norm or l1-norm methods. Traditional algorithms optimize the calculation by minimizing L2-norm and introducing 'smoothness', including Newton One Step Error Reconstruction (NOSER) [2], Tikhonov regularization [3], Laplacian regularization [4], the Landweber Iteration method [5]. L1-norm based method known as Total variation methods, and various methods, such as, PDIPM [6], LADMM [6], Split Bregman [6], and developed to solve such a non-differentiable functional. L1 regularization is difficult, however, it is chasing piecewise constant by imposing sparsity, and helpful for preserving the sharp boundary of the target under tested. For monitoring purpose, reconstructing high-quality images is always the target. Previous works suggest that TV has the capability to produce sharp-edged images and preserve the discontinuities between the background medium and the target and is especially suitable for big contrasts. The TV regularization method was firstly proposed by L.I. Rudin and S. Osher in 1992 as a denoising algorithm [7]. In comparison, the conventional least-square method uses the L2-norm yields linear solutions and can be computed with an algebraic framework, whilst TV employing L1-norm is nonlinear and computationally complicated, however, research shows that TV functions makes contributions to edge preserving, and becomes an appropriate method for noise removal and deals with image restoration. TV regularization has received much attention, especially in electrical tomography in recent years. Strickly speaking it is worth mensioning that the TV method is, in some level, linked well with l1-norm method, but they are theoretically different from each other. The TV starts from the block prior assumption, while the l1-norm starts from the sparse prior assumption.

EIT sensors have a few different types, depending on the way of accessing data, and the availability of where data could be measured. Circular EIT is commonly applied to relatively flexible situations where most sides of the region of interest are accessible, for example, an electrode ring could be installed on the wall of the entire pipeline for monitoring purposes. However, some cases would have limitations and inconveniences in data collection, where only a single side would be available for measurement, for instance, some inclusions buried in the ground or inside water that only the surface would be available for data acquisition. The circular electrode model would not be suitable for any such circumstance, and a planar array installed on a subsurface EIT sensor would potentially be helpful for visualizing the target. Subsurface EIT is similar to a 'scanner' for 3D visualization and can be useful in various applications, however, it would suffer from additional challenges, especially in cases where samples are placed very deep. Current density and the strength of electric fields would decay with the distance from the subsurface electrode-plane, and extra difficulties are imposing if inclusion leaving far from the planar array. However, compared with the planar array and dual-plane sensor for EIT visualization of a pipeline, a conventional circular electrode-plane could represent the spatial information of the whole medium of interest, but would suffer from a very low resolution along axis-directions because of the limited number

of rings. Although multiple electrode-plane sensors have shown improvements in spatial resolution, it would also place a high demand on the data acquisition system since many more electrodes will be involved. Planar array can provide assistance in exploring information of the region with less depth. Although the center area might be difficult to detect (but also depending on the size of the pipeline and planar array), it still capable of generating 3D images with higher resolution on axis-direction in its detectable region, which supplements the traditional EIT model using electrode rings around the pipeline. In this case, a planar array could potentially be combined with a traditional ring model to produce more useful information.

Subsurface EIT has been studied mostly in clinical applications. In 2000, J.L. Mueller presented their work, in which a rectangular electrode array based on EIT was applied to the human chest for 3D reconstruction during ventilation and perfusion, suggesting the potential for collecting information about blood volume variations in the chest [8]. Following on from that, other clinical applications have also been shown in the last decade, such as in, prostate disease [9], and cervical neoplasia [10]. More recently, H. Perez presented a method for 3D image reconstruction using a novel electrode configuration in the context of breast cancer, where electrodes of current injection and voltage measurement work separately [11] .EIT using planar array is actually different with the conventional ones with electrode bounded the whole region of interest if the domain of interest is infinite (such as ground), and such approach can also termed open domain EIT since all electrodes are placed on one side, which introduces more challenges on image reconstruction. To overcome such an effect, most research approximates it to be an enclosed domain, but this brings error, and a recent study proposed to transform the original open domain into an enclosed 2D circular domain based on Riemann mapping [12].

In this work, we are aiming to explore the flow visualization approach using a planar array with the EIT approach, in addition, numerical measurements of target depths based on reconstructed images are studied. Split Bregman TV regularization has been chosen for visualization to test the performance of subsurface EIT, and both simulation and experiments are included in this work. Simulation is implemented by modelling a phantom with a 4×4 electrode planar array on the top surface to demonstrate the feasibility of the approach, and the experimental sensor was designed, keeping it consistent with the simulated model, in which a series of experiments are validated. Moreover, position error and volume fraction are applied for assessing the image quality, and suggested parameter selection method. Furthermore, results based on selected parameters using real data are displayed, and spatial gradients along the depth were generated for working out the depths that reflected visualized images. The accuracy of the depth detection of the samples is shown and discussed.

II. Mathematical Model of EIT

A typical EIT system is composed with data collection system, software system and a sensor with region of interest. Measurement data are collected via electrodes that attached on the boundary of the region, and conductivity distribution is expected to get recovered by solving forward and inverse problem. Forward problem of EIT is aiming at determining potential distribution throughout the interested region. The starting point is deriving Maxwell's equations [13], and the forward problem under low-frequency assumption can be described by:

$$\nabla \cdot \sigma \nabla u = 0 \qquad (1)$$

Where u is electrical potential in region of imaging and σ is electrical conductivity in sensing domain. The current density j is generated via electrodes while current excitation conducted [14]. Imposing the boundary condition with normal vector $\vec{n}$, current density j is given by:

$$j = \sigma \frac{\partial u}{\partial \vec{n}} \qquad (2)$$

A complete electrode model involves relationships with boundary potential and contact impedance [15] [16], which described with:

$$u + z_l . \sigma \frac{\partial u}{\partial \vec{n}} = v_l \qquad (3)$$

Where z_l is contact impedance and v_l the electric voltage of current carrying electrode. In this paper, difference imaging EIT is conducted, where potential difference Δu is measured on electrode, and reconstructed image is visualizing a mapping of $\Delta\sigma$. A forward equation is described with Jacobian matrix [17]:

$$\Delta u = J \cdot \Delta\sigma \qquad (4)$$

Where J donates the Jacobian matrix, defined as $\frac{\delta u}{\delta \sigma}$.

Figure 1 is showing a FEM mesh of simulated planar array using EIDORS software. Figure 2 represents a normalized background data of simulation and experiment, and they are matched each other. Sensitivity map produced by Mayavi software is displaying in figure 3, which suggests that the sensitivity is reduced with distance.

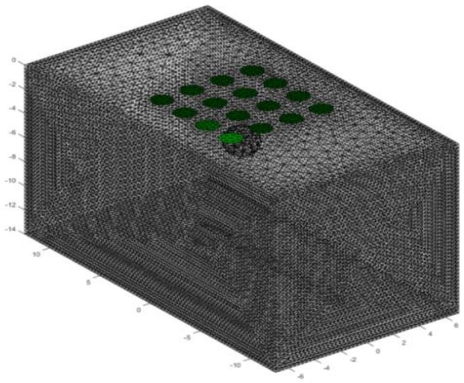

Figure 1: Forward modeling of planar array using EIDORS

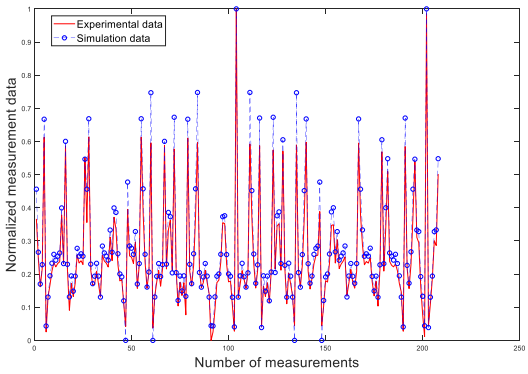

Figure 2: Comparison of normalized background data from simulation and experiment with EIT Planar Array

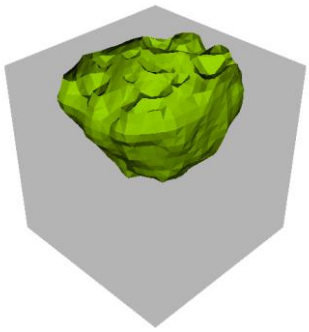

Figure 3: Sensitivity mapping of Planar Array drawing by Mayavi

Inverse problem is solving $\Delta\sigma$ with calculated potential distribution determined by FEM forward solver, which is an ill-posed problem. Regularization algorithms are developed for overcoming such an optimizing problem. In this paper, Split Bregman (SB) TV is employed for image reconstructions using planar array EIT. The constrained optimization problem of ERT with SB is:

$$\Delta\sigma = argmin_{\Delta\sigma}\|\nabla\Delta\sigma\|_1 \ \ s.t. \|J\Delta\sigma - \Delta u\|_2^2 < \delta \qquad (5)$$

This equation can be solved by imposing Bregman iteration technique [19]. The iterative equations of SB [19] [20] are:

$$(\Delta\sigma^{k+1}, d^{k+1}) = argmin_{\Delta\sigma}\{\frac{\mu}{2}\|J\Delta\sigma - \Delta u\|_2^2 + \|d\|_1 + \frac{\lambda}{2}\|d - \nabla\Delta\sigma - b^k\|_2^2\} \qquad (6)$$

$$b^{k+1} = b^k + \nabla\Delta\sigma^{k+1} - d^{k+1} \qquad (7)$$

III. METHOD

a. *Image-based depth detection*

The depth of the target is detectable based on the 3D reconstructed image of EIT. There are two different depths defined. The distance between the CoG of the target and planar array is labelled D_c, and the distance D_t measures the distance from the top surface of the target to the planar array. Calculation of D_c is given by working out the CoG of target based on visualization. The distance D_t is measured with an average distance since the 3D image produced by EIT would not be perfect, so it is more accurate to discover the depth D_t of the target from different points from the top boundary os the 3D image. Note that the 3D images are composed with voxels of $21 \times 21 \times 21$, so the distance can be detected by searching downward from a voxel on the top slice through voxels of 1×21. In this chapter, a 2D slice is extracted from the center, and 3 lines of voxels in the center are taken out for calculations of average distance, where

$$D_t = \frac{1}{3}(D_1 + D_2 + D_3) \qquad (8)$$

b. *Numerical analysis*

In some literature, void fraction would commonly be utilized for analysis of the reconstructed result. In the two-phase, void fraction is defined as the ratio between the disperse phase and continuous phase. In terms of the static experiments that have been conducted in this paper, a similar definition is given, where the fraction of the 3D object (Volume fraction) is defined as the effective volume ratio between the inclusion and the conductive region in 3D phantom. To evaluate the results that are generated using a planar array based on the SBTV algorithm, the error of volume is taken into account for the numerical analysis. The true volume of the target is 15.625 cm^3, and the calculation of the volume of the tested sample is given by the thresholding images. The numerical analysis of volume fraction uses the average relative error of volume (REV):

$$\text{REV} = \text{ave}\left(\frac{|V_{IMAGE} - V_{true}|}{V_{true}} \times 100\%\right) \qquad (9)$$

In many industrial or geophysical applications, the detection aimed at an unknown object in a region of interest is very important, where knowledge of the depth of the detected object can potentially be suggested by reconstructed images from Subsurface EIT using a Planar Array sensor. Therefore, numerical analysis of position error aimed at depth detection is critical. Paying attention to the detected depth of the target, the calculation of the Centre of Mass of an image can reflect depth D_C, and the residual error is given by the numerical difference of the depth from reconstructed image and the actual depth. The numerical analysis of the performance of depth detection with subsurface EIT employed average relative error (RED):

$$\text{RED} = \text{ave}\left(\frac{|D_{IMAGE} - D_{true}|}{D_{true}} \times 100\%\right) \qquad (10)$$

c. *Parameter selection*

Although some studies have shown that the SBTV algorithm contributes to improving the image quality, different combinations of parameters can largely affect the result of either visualization or numerical measurements that reflected from reconstructed 3D images. Such situations also create a fluctuating residual error which leads to uncertainty if optimal parameters cannot be discovered. In addition, the number of parameters, as in the case of SBTV algorithm with three parameters, also brings more difficulties as so many combinations of parameters make it too hard to make choices. In such situations, numerical analysis would be helpful for making the selections of parameters. In the iteration schemes of SBTV algorithm that has been used in this chapter, three

parameters, μ, λ and γ, are involved in the iterative calculations. If optimal parameter selection can be made using a training procedure, and those selected optimal parameters are brought for further testing, it would be helpful for effectively solving the inverse problem. The main idea of parameter selection is choosing those close to the ideal solution, and a range of relative error is set up for discovering qualified solutions among lots of parameter combinations. For detection purposes using an EIT planar array, the numerical depth and size of reconstructed object were paid close attention. The true depth and volume are calculated as the expected 'ideal' solution. There were 3375 combinations of parameters produced for 'training', where each set of parameters has a corresponding image. The depth and volume can quantitatively be determined from reconstructed 3D images, which give a residual error between the solution and the true measurement. If their corresponding error is located within the defined range they are considered as optimal parameters. The parameter selection process requires the following scheme:

IV. SIMULATION TESTS

The 3D modelling of EIT using Planar Array has been simulated based on EIDORS. The phantom was designed as a cubic tank with a 16 (4×4) circular electrode-plane placed single sided. The background medium has been given a conductivity of 1, while a sphere with various locations and depth as an inclusion with a conductivity of 10. Excitation current was set at 0.1 mA, and the current pattern has been chosen as a neighboring excitation and measurement method. Figure 1 displayed below shows the forward modelling of such a planar array, and the specifications of sizes of different components of the model are illustrated in Table 1. In the 3D coordinate system, the subsurface EIT model is defined within the range of $-7cm < x < 7cm, -12.5\ cm < y < 12.5\ cm, -14\ cm < z < 0$, with the geometrical centre of the electrode-plane being located at the origin of coordinates $(0, 0, 0)$. In this section, different locations with varying depths of the sample are set-up for the simulation test, and reconstructed images are displayed in Figure 4.

Table 1: Specifications of simulation phantom of Planar Array

Items	**Size**
Number of electrodes	16
Length	25cm
Width	14cm
Depth	14cm
Diameter of circular electrodes	0.85cm

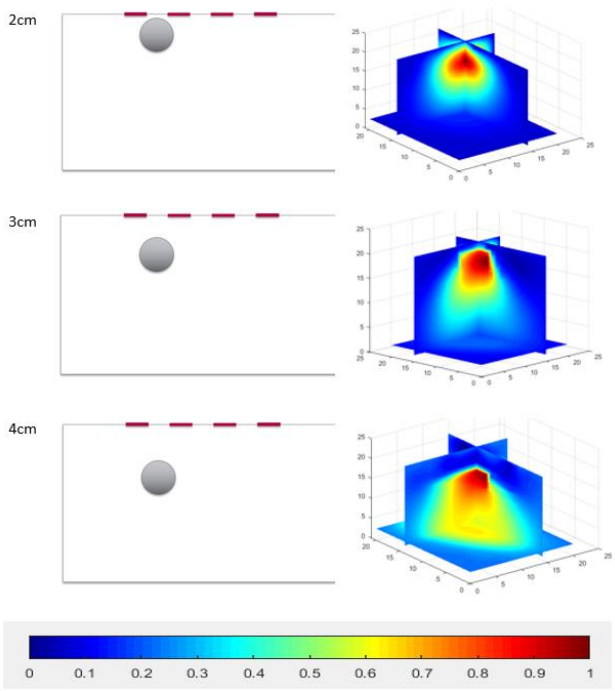

Figure 4: image reconstructions of simulation test in different depth

Depths of 2cm, 3cm, and 4cm have been chosen as distances between the center of the target and the planar array to make detections based on the shape of the sensitivity map. The simulated sample was placed at different positions with 3 different depths. In Figure 4, detections with simulation of center position are conducted, and the visualization results are displayed with corresponding true images placed on the left-hand side. According to the results shown in the figure above, visualizations produced using a planar array show consistence in various locations. At different depths of each location, the reconstructed 3D objects are showing agreement on tendency, with changes in the distance between the object's top surface and electrode-plane being recognized.

Since images are reconstructed from targets that are placed at different positions and depths, the numerical depths explored should be feasible based on visualized results using the TV algorithms with optimal parameters. If the depth is measured from the planar array to the center of the object, the Centre of Mass (CoM) of the recovered 3D object can be calculated based on the thresholding image. Results of the depth measurement based on visualization are shown below:

Table 2: Detected depth of different locations from simulation tests.

Locations\True Depth	2cm	3cm	4cm
Center	2.0328cm	3.0167cm	4.032cm
Left	2.078cm	3.037cm	4.11cm
Right	1.922cm	3.03cm	3.78cm

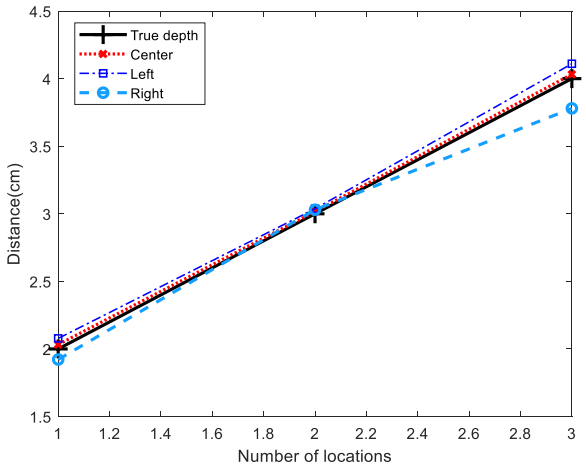

Figure 5: Plots of reflected distance D_c of the target from images based on simulation

In terms of the image quality before quantitative analysis, all images are showing a sharp edge on the top surface, and the other side is very smooth. Degraded 3D images are observed since the volume gets bigger as the distance moves further down. Theoretically, reconstructed image can suggest the detected distance. Numerical calculations of distance detected by EIT planar array based on simulation data are represented, and Figure 5 brings them together as line graphs to make a comparison. The black line indicates the true distance, and others are given by the quantitative results that are suggested from positions that have been tested in the simulation. Regarding these numerical distances, results from all positions are showing a better performance with 2cm and 3cm, while it starts to degrade at the depth of 4cm. Comparing the different positions, the one at the center of the planar array gives a slightly better result as the calculated distance is closer to the true distance, with the others showing a little further deviation. In general, the simulation results display a successful visualization as well as providing the quantitative measurement result of depth detection, which suggests that it would be feasible to explore information based on 3D EIT using a planar array. In the next section, experiments using a phantom are engaged to validate this idea.

V. Experimental Validation and Results

Conductivity mapping across the region of interest would theoretically be re-distributed if the inclusion changed the locations or depth, therefore Subsurface EIT could potentially be applied to detecting or monitoring an invisible and unknown sample underneath a surface with real data. The previous section has shown reconstructed images with the sample at different depths and locations using simulation data, and compared detected distance based on visualization, which quantitatively showed agreement with the true distance, hence demonstrating the feasibility of sample detection using subsurface EIT. In this section, experimental validation has been engaged based on real experimental data collected from a designed Planar Array sensor. The main body of the designed physical planar array sensor for experiments is made from a transparent cubic tank with the electrode plane on the front surface, enabling it to contact the medium inside the tank. The size of the tank is $14\,\text{cm(length)} \times 14\,\text{cm(width)} \times 25\text{cm(height)}$, and the 4×4 electrode-plane is fixed with a diameter of 0.85cm for all the circular electrodes. The EIT Swisstom Pioneer system [21] has been utilized for data collection, where a current with an amplitude of 1mA and frequency of 195 KHz has been chosen as the excitation source. The experimental sensor was designed to be consistent with the simulation model. A metal cube with a size of $2.5\text{ cm} \times 2.5\text{ cm} \times 2.5\text{ cm}$ was chosen as a testing sample in a series of experimental tests, and tap water filled the tank as a background conductive liquid. Background measurement data using a planar array sensor is compared with simulation data, and Figure 2 shows consistent agreement with measurement data.

Position and depth tests are applied in this section, where the target has been placed at different positions and depths for each test. To simplify the illustration of each location of the sample, the region has been divided into a few areas. The top-view of the sensor has a 3×3 grid formed by the 16 electrodes, and each area could be renamed (for simplified description) as: Middle-left (ML), Middle-right (MR), Centre (C), Upper-left (UL), Upper-middle (UM), Upper-right, Lower-left (LL), Lower-middle (LM), Lower-right (LR).

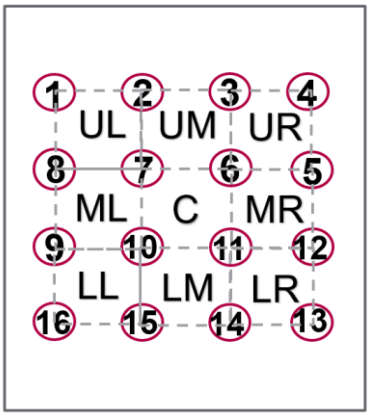

Figure 6: Simplified drawing of Subsurface ERT sensor

a. Position and depth detections

Above all, the capability of detecting different positions underneath the planar array is investigated. The metal cube has been placed at 6 positions with the same depth. In order to produce good quality images using the experimental data, some quantitative parameters defined in section III(b) are conducted for the purpose of selecting optimal parameters to be involved in the SBTV algorithm. The procedure of parameter selection was presented in section III(c) in detail.

The SBTV algorithm has three parameters. The choice of the parameter can largely affect the reconstruction results when using TV regularization, and the residual error in numerical depth and volume are largely fluctuating. Experiments have been conducted with various combinations of parameters, and results of numerical depth and volume of the imaged target are largely varying. Some results are actually very far from the truth and bias the expected result. Hence, parameters should be optimized to obtain expected results. Manual parameter selection would require experts who are familiar with the TV algorithm and have knowledge of how each parameter would affect the image. However, TV

regularisation is complicated, and such work would be time-consuming, and there were no much works suggesting how each parameter influence the reconstructions.

Parameter selection in this paper was manipulated using the procedure stated in the last section, where results with residual errors under 10% are considered acceptable. Results in Table 3 shows that relative error in the volume calculation of the target could be controlled to around 5% in all positions and different depths, which lead to the numerical error being about 0.78 cm^3. In depth detection (Table 4), the average residual error of the tested depth of up to 3cm could be controlled to be 0 on average. For the depth of 4cm, the error in the center is slightly lower than other locations, and results located in the corners are showing a higher average relative error. However, for the planar array sensor that is employed in these experiments, the depth of 4cm is generally the detectable limit, since measurements would not react to further distances for such a small sensor and target, and such numerical analyses indicate the consistence between the result and the sensitivity mapping. A series of experiments were conducted with the metal target hanging at positions of center and corners with depths of 2cm, 3cm and 4cm measured from the center.

Table 3: Numerical analysis of errors of reconstructed sample volume with respect to actual volume of 15.625 cm^3

Depth/error/ locations		UL	UM	UR	ML	Center	MR
2cm	Volume / REV	15.38cm^3/ 4.96%	15.56cm^3/ 4.80%	15.95cm^3/ 5.70%	15.82cm^3/ 5.66%	16.18cm^3/ 6.5%	15.63cm^3/ 5.28%
3cm	volume / REV	15.849cm^3 /5.10%	15.825cm^3 /4.54%	15.575cm^3 /5.74%	15.858cm^3 /5.7%	15.790cm^3 / 5.47%	16.445cm^3 /6.8%
4cm	volume / REV	16.169cm^3 /6.83%	16.402cm^3 /6.66%	15.814cm^3 /5.44%	16.400cm^3 /5.0%	16.100cm^3 /6.09%	15.997cm^3 /5.05%

Table 4: Numerical analysis of position errors of reconstructed sample with respect to actual depth

Depth/error/locations		UL	UM	UR	ML	Center	MR
2 cm	Depth / RED (%)	2cm/0%	2cm/0%	2cm/0%	2cm/0%	2cm/0%	2cm/0%
3 cm	Depth / RED (%)	3cm/0%	3cm/0%	3cm/0%	3cm/0%	3cm/0%	3cm/0%
4 cm	Depth / RED (%)	3.745cm/ 6.80%	3.778cm/ 6.23%	3.916cm/ 5.61%	3.859cm/ 5.62%	3.792cm/ 5.28%	3.816cm/ 5.66%

Table 5: Experimental tests with multiple samples. All inclusions are placed with same depth.

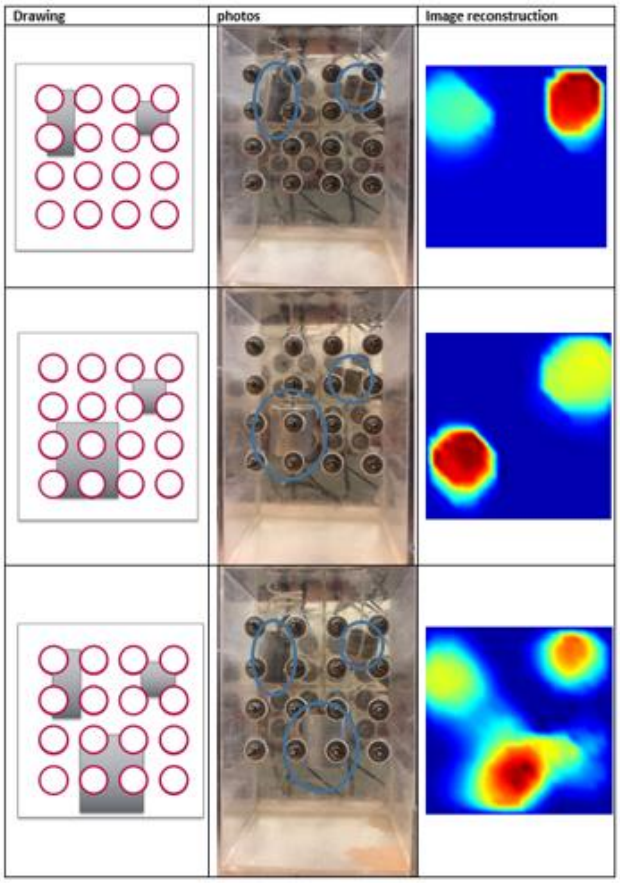

According to many experimental tests, it was discovered that optimized parameters based on volume fraction/ depth might not be the optimal combinations for detecting precise depth/ volume. In other words, the position error could still be large or over the expected standard although the volume is very close to the actual size of the tested sample, or ones with accurate depth might have an enlarged/shrunken volume of the target. For solving such a problem, joint constraints for training can be made to find out an 'overlapping' that satisfies both conditions. For detection purposes, the position error is a more important factor, the implement of reconstruction is conducted by priory ensure a good accuracy of the position. Figure 7 represents the reconstructed 3D images using optimized TV parameters.

Table 6 Experimental tests with a single sample placed at different positions with the same depth.

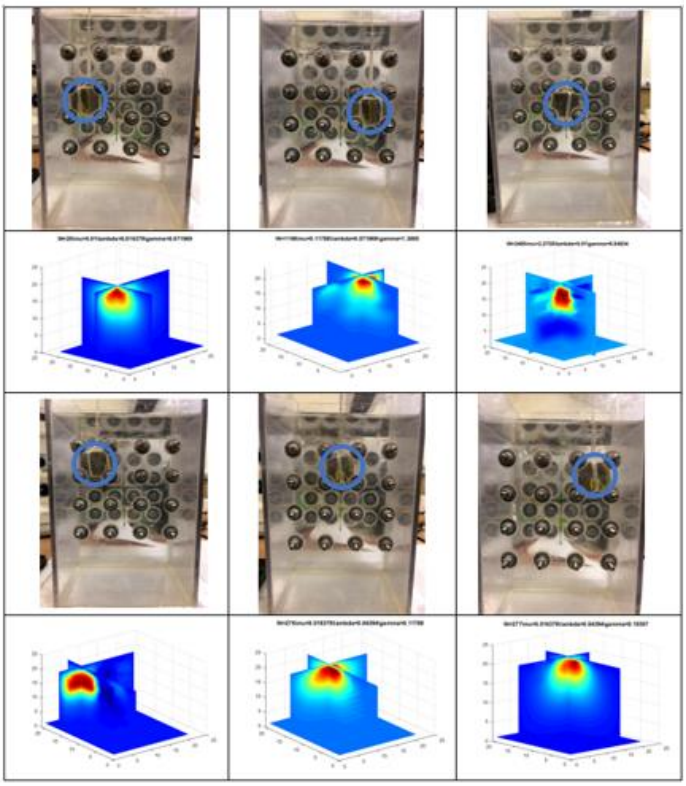

Table 5 indicating the performance of planar array on testing multiple inclusions. The samples with different size are placed at the same distance to the array. Table 6 is displaying the results of the positions tests with single inclusion. It is suggested that all inclusions are properly monitored. In terms of multiple-inclusion tests, the results are showing that the sample with the bigger size is dominated the visualized results, in this case, different inclusions are recognizable. Image reconstructions of depth detection tests are showing in table 7, where the sample is placed at a different distance to the planar array. Images indicate that the recovered object on the visualized result is moving down with the sample placed further. In terms of image quality, it could be found that the top surface of the object is sharp, whilst the bottom side is still blurred. This might mean that it is suffering from data miss on the other side of the inclusion, where there are totally no electrodes for data acquisition. To support such a conclusion, the comparison works with Tikhonov algorithm as well as numerical analysis of depth detection are illustrated in the next section.

Table 7: Image reconstruction of depth detection. Various depth was applied to each set with the metal cubic inclusion parallel to the center of the electrode plane. Note that the electrode array on the left surface of the tank was connected for experimental tests.

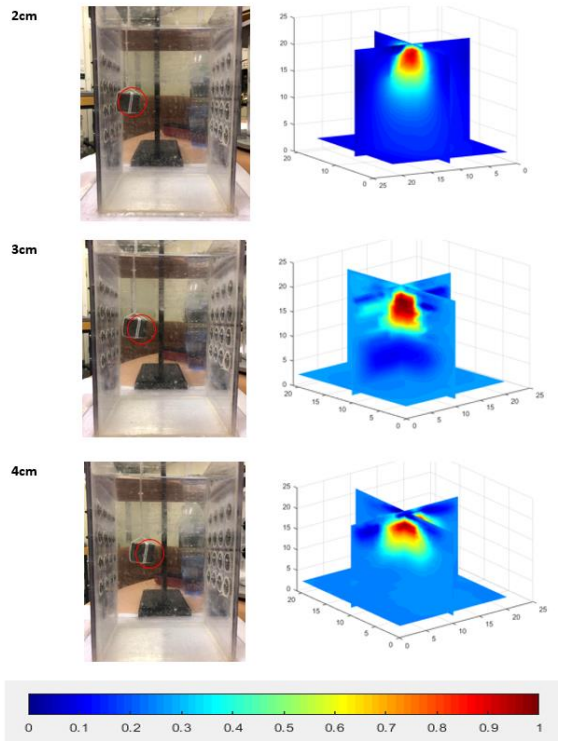

b. Analysis of gradient

In figure 8, a comparison work is displayed, where the visualization results on the sample with different distance to the planar array are compared between SBTV and Tikhonov algorithm. The results that using TV have a sharp top boundary and blurred on the other side. Visualizations of subsurface EIT in Figure 8 show the results by using optimized parameters with new experimental sampling data at different depths. In comparison, images have blurred whole boundary with use of Tikhonov method. In addition, results of TV can show consistence to a different depth, whilst Tikhonov can hardly recognize the distance.

Since the TV algorithm can reconstruct an image with a sharp top boundary, the reconstructed image can reflect the distance of the tested sample by plotting spatial gradient. The spatial gradient is given by the difference in conductivity distribution along the direction of interest. Smooth distributions would indicate a slow stepping up/down, while a sharp gradient suggests a sharp boundary. Spatial gradient (in the direction of depth) is capable of discovering where the upper boundary of the object located, which reflects the distance measured from the top-surface to the electrode-plane. Based on the results that demonstrated in Figure 8 that using TV algorithm, distance measurement results based on images reconstructions are showing in figure 9.

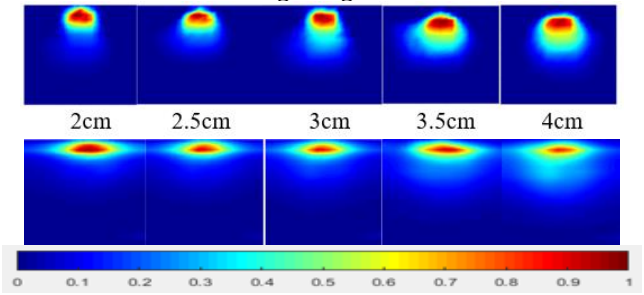

Figure 8: Visualization results of center position with various detection depth. Images on the top and bottom are reconstructed using TV and Tikhonov respectively.

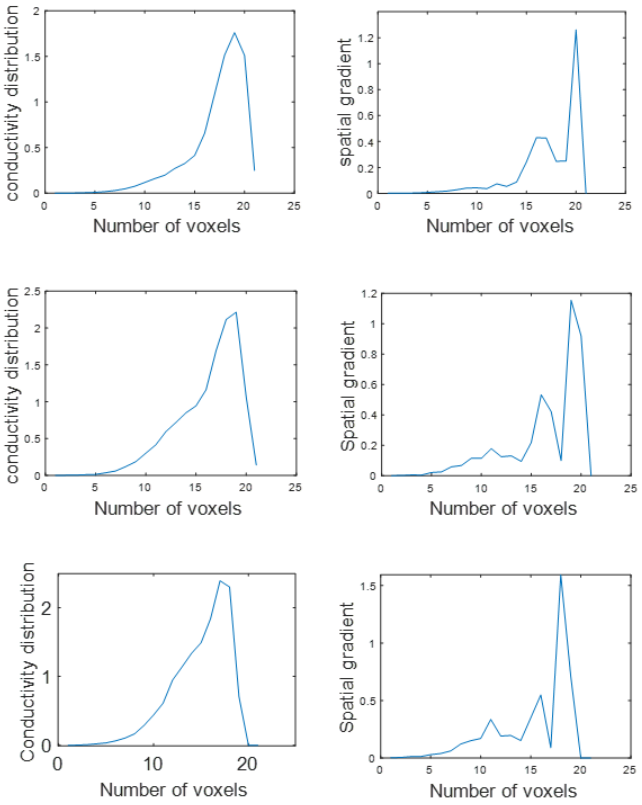

Figure 9: Distance measurement results based on images reconstructions with TV algorithm reflected by spatial gradient on 2cm, 3cm and 4cm

Figure 9 displays the spatial distribution conductivity values against the number of elements, where the reconstructed 3D image is composed of 21× 21 × 21 voxels. From the spatial distribution graphs, the growing tendency at the beginning is very smooth and steady and has a sharp change at the end. Such a result suggests the change of the sharpness along the direction of interest. The part before and after the peak point corresponds to the area underneath and above the top-boundary on reconstructed images. Sharpness on the top is far more than the region below the sample, this clarifies the truth that more information of the area near the top surface is recorded by electrodes, whilst missing data, as well as a weakened electric field on the other side, lead to a smoothing object boundary on reconstructed images. The absolute gradient demonstrates how fast the conductivity distribution varies along the plotted direction. The maximum peak value estimates the location of the upper boundary, and the corresponding pixel number on the 2D slice could be read from the x-axis, which is related to the distance between the upper boundary and the subsurface sensor. Results suggest the accuracy of measuring distance using this method, and more error would be introduced with further distance to the planar-array due to image quality degradation. Numerical results show an accuracy of 89.3%-72.7% when the distance went from 2cm to 4cm. The number of elements that are setting up the reconstructed 3D images is actually limited for the purpose of saving computational time, and a 2D cross-sectional slice from the 3D image only contains 441 elements. Along the direction of depth, the limit number of elements may lead to degraded accuracy in calculations of distance. For the application stage in the future, an improvement in the element number would potentially contribute to a more precise measurement based on image reconstruction. In this study a traditional neighboring electrode arrangement and a 4 x 4 matrix based electrode set up was used. Excitation pattern and electrode arrangement will have an important impact on quality of images from planar array imaging, as shown in previous similar studies [11], [18]. Such an optimization for electrode arrangement and/or excitation patter can produce overall sensitivity that could enhance the detection depth and other image quality parameters in planar array.

VI. Conclusion

EIT is a visualization technique that produces images based on a sensitivity map and measurement data from electrodes in contact with a region of interest. Applications that use EIT can benefit from its features of high time resolution, low cost, and non-invasive. However, the inverse problem of EIT is ill-posed, and reconstructed images suffer from a low spatial resolution, especially in the cases of missing data. Subsurface EIT has been researched for several decades. It is still a challenging problem despite many efforts has been put into many applications since the image quality might be degraded due to decaying of the current density on the region with deep distance. To detecting the depth of the targets, it is required to optimize the image quality, as a perfect image could reflect numerical parameter measurements. Total variation is capable of preserving the edge of the detected targets, although EIT planar array sensors suffer from data missing on the other side, a sharp boundary on the top surface is successfully observed. The visualized information of the target topside is more critical while the bottom may be less important for sample detection purposes. Therefore, utilization of the TV algorithm can improve the image quality and spatial resolution of EIT reconstructed images, and visualizations of conductive objects in pipelines with EIT has great potential. In this chapter, the capability of the planar array has been investigated using a series of simulation and experimental phantom tests. Simulation has shown the feasibility of depth detection using an EIT planar array, and experiments have been carried out based on the simulation modelling. Visualization results employing Split Bregman TV have been shown and discussed, where few quantitative parameters are defined for evaluating reconstructed images. In addition, a simple method has been suggested to select parameters aiming at producing qualified images. The imaging results showing that an EIT planar array with an overall size of 4.5cm×4.5cm could monitor to a depth of around 4cm, with a depth detection accuracy of up to 89.3%.

VII. Bibliography

[1] Santosa, F. and Vogelius, M. “A Backprojection Algorithm for Electrical Impedance Imaging. ”, SIAM Journal on Applied Mathematics, 50(1), pp.216-243. 1990.

[2] M.Cheney,D.Isaacson,J.C.Newell,S.Simake,and J.Goble,"Noser: An algorithm for solving the inverse conductivity problem," Int. J. Imag. Syst. Technol., vol. 2, pp. 66–75, 1990.

[3] Vauhkonen, M., Vadasz, D., Karjalainen, P., Somersalo, E. and Kaipio, J., " Tikhonov regularization and prior information in electrical impedance tomography. ", IEEE Transactions on Medical Imaging, 17(2), pp.285-293. 1998.

[4] B. Brandstatter, G. Holler, and D. Watzenig. "Reconstruction of inhomogeneities in fliuids by means of capacitance tomography. ", COMPEL: The international Journal for Computation and Mathematics in Electrical and Electronic Engineering, 22(3): 508-519, 2003.

[5] Li, Y. and Yang, W., " Image reconstruction by nonlinear Landweber iteration for complicated distributions. ", Measurement Science and Technology, 19(9), p.094014. 2008.

[6] Andersen K D, Christiansen E, Conn A R and Overton M L, "An efficient primal-dual interior-point method for minimizing a sum of euclidean norms", SIAM J. Sci. Comput. 22 243–62, 1999.

[7] Rudin, L., Osher, S. and Fatemi, E., " Nonlinear total variation based noise removal algorithms. ", Physica D: Nonlinear Phenomena, 60(1-4), pp.259-268. 1992.

[8] J.L. Mueller, D. Isaacson, and J.C. Newell, "Reconstruction of conductivity changes due to ventilation and perfusion from EIT data collected on a rectangular electrode array," Physiol. Meas., vol. 22, no. 1, pp. 97-106, 2001.".

[9] A. Borsic, R. Halter, Y Wan, A Hartov, and K.D. Paulsen, "Electrical impedance tomography reconstruction for three-dimensional imaging of the prostate," Physiol. Meas., vol. 31, no. 8, pp. S1-S16, 2010.".

[10] V A Cherepenin, Y V Gulyaev, A V Korjenevsky, S A Sapetsky, and T S Tuykin, "An electrical impedance tomography system for gynecological application GIT with a tiny electrode array," Physiol. Meas., vol. 33, no. 5, pp. 849-862, 2012.".

[11] H. Perez, M. Pidcock, and C. Sebu, "A three-dimensional image reconstruction algorithm for electrical impedance tomography using planar electrode arrays," Inverse Probl. Sci. En., vol. 25, no. 4, pp. 471-491, 2017.

[12] Wang, Y., Ren, S. and Dong, F. , "A Transformation-Domain Image Reconstruction Method for Open Electrical Impedance Tomography Based on Conformal Mapping. ", IEEE Sensors Journal, 19(5), pp.1873-1883. 2019.

[13] Holder, D. "Electrical impedance tomography: Methods, History and Applications." ,London: Institute of Physics, p.23. 2005.

[14] Silvera-Tawil, D., Rye, D., Soleimani, M., & Velonaki, M. "Electrical Impedance Tomography for Artificial Sensitive Robotic Skin: A Review. " , Sensors Journal, IEEE, 15(4), 2001-2016, 2015.

[15] Somersalo, E., Cheney, M. and Isaacson, D. "Existence and Uniqueness for Electrode Models for Electric Current Computed Tomography. " SIAM Journal on Applied Mathematics, 52(4), pp.1023-1040.1992.

[16] K-S. Cheng, D. Isaacson, J. C. Newell, and D. G. Gisser, "Electrode models for electric current computed tomography, " IEEE Trans. Biomed. Eng., vol. 36, no. 9, pp. 918-924, 1989.

[17] Polydorides N and Lionheart W R B, " A Matlab toolkit for three-dimensional electrical impedance tomography: a contribution to the Electrical Impedance and Diffuse Optical Reconstruction Software project." Meas. Sci. Technol. 13 1871–1883., 2002

[18] Tholin-Chittenden C, Soleimani M, "Planar Array Capacitive Imaging Sensor Design Optimization." IEEE Sensors Journal, vol. 17, no. 24, 2017.

[19] Goldstein, T.; Osher, S. "The Split Bregman Method for L1-Regularized Problems. " SIAM J. Imaging Sci., 2, 323–343., 2009.

[20] Li, F., Abascal, J., Desco, M. and Soleimani, M. "Total Variation Regularization With Split Bregman-Based Method in Magnetic Induction Tomography Using Experimental Data. " IEEE Sensors Journal, 17(4), pp.976-985., 2017.

[21] "EIT Technology." Swisstom. Available online: www.swisstom.com/en/eit-technology-3 (accessed on 13 March 2019).," [Online].

[22] X. Song, Y. Xu, F. Dong. " A spatially adaptive total variation regularization method for electrical resistance tomography'' Meas. Sci. Technol. 26, 125401 (15pp), 2015.

[23] Zhou Z, Gustavo Santos G S, Dowrick T, Avery J, Sun Z, Xu H and Holder DS. "Comparison of Total Variation Algorithms for Electrical Impedance Tomography." Physiological Measurement, vol. 36, no. 6, pp. 1193–1209, 2015.